Negative Differential Resistance in van der Waals Heterostructures Due to Moiré-Induced Spectral Reconstruction

Damien J. Leech,[1] Joshua J. P. Thompson,[1,*] and Marcin Mucha-Kruczyński[1,2]

[1] *Department of Physics, University of Bath, Claverton Down, Bath BA2 7AY, United Kingdom*
[2] *Centre for Nanoscience and Nanotechnology, University of Bath, Claverton Down, Bath BA2 7AY, United Kingdom*

(Received 14 March 2018; revised manuscript received 6 June 2018; published 7 September 2018)

Formation of moiré superlattices is common in van der Waals heterostructures as a result of the mismatch between lattice constants and misalignment of crystallographic directions of the constituent two-dimensional crystals. Here we discuss theoretically electron transport in a van der Waals tunneling transistor in which one or both of the electrodes are made of two crystals forming a moiré superlattice at their interface. As a proof of concept, we investigate structures containing either an aligned graphene/hexagonal boron nitride heterostructure or twisted-bilayer graphene and show that negative differential resistance is possible in such transistors and that this arises as a consequence of the superlattice-induced changes in the electronic density of states and without the need for momentum-conserving tunneling present in high-quality exfoliated devices. We extend this concept to a device with electrodes consisting of aligned graphene on α-In_2Te_2 and demonstrate negative-differential-resistance peak-to-valley ratios of approximately 10.

DOI: 10.1103/PhysRevApplied.10.034014

I. INTRODUCTION

The phenomenon of negative differential resistance (NDR) is a striking example of nonlinearities in physics: within a certain region of the current-voltage characteristic of a device, increase of applied voltage leads to decrease of the output current. In the first solid-state device displaying NDR, the Esaki diode [1], this effect arises because increasing bias voltage modifies alignment of the occupied and empty electronic states in the source and drain electrodes separated by a tunneling barrier. At zero and large bias, due to either the lack of occupied states at the source or empty states at the drain, this alignment prohibits flow of current. In contrast, within a certain bias window in between these two cases, the positioning of energy levels allows electrons to tunnel through the barrier.

More recently, NDR was observed in van der Waals (vdW) heterostructures of two-dimensional atomic crystals as a result of momentum-conserving electron tunneling through an atomically thin barrier [2–7]. Because of the high quality of the crystals produced by mechanical exfoliation and the atomically sharp interfaces in the assembled vdW-coupled stack [8], the requirement to match both the energy and the momentum of the initial and final states leads to a peak in the tunneling current as applied voltages tune the source and drain to a particular band alignment. However, exfoliation, while providing state-of-the-art materials and devices, is not a scalable fabrication method. At the same time, materials produced by other methods, such as chemical vapor deposition, do not achieve the quality necessary to observe momentum-conserving tunneling and seemingly NDR [9,10].

Here we show theoretically that NDR can be achieved in vdW heterostructures without momentum-conserving tunneling. We exploit modifications of the electronic band structure of such heterostructures due to the interplay between lattice constants as well as misalignment of the crystallographic axes of two neighboring layers, which lead to the formation of a superlattice at the interface. This superlattice is commonly referred to as the “moiré pattern” and is unique to vdW heterostructures, in which, due to the vdW coupling between different materials, lattice matching is not necessary for the whole structure to be stable. Crucially, formation of the moiré superlattice is often accompanied by reconstruction of the electronic band structure as the moiré periodicity folds the dispersion into minibands. This results in the opening of minigaps at the boundary of the superlattice Brillouin zone and the appearance of Van Hove singularities in the electronic density of states (DOS) [11–22]. We simulate the tunneling current in two common vdW heterostructures in which the source electrode is either (1) monolayer graphene highly aligned with underlying hexagonal boron nitride (hBN) or

*j.j.p.Thompson@bath.ac.uk

 © 2018 American Physical Society

(2) twisted-bilayer graphene (tBLG) and show that moiré-induced spectral reconstruction can result in NDR. We then study a more-complex device with both the source electrode and the drain electrode made of a moiré-forming stack. We show that in the case of graphene/α-In_2Te_2 electrodes, NDR an order of magnitude larger than for the two previous architectures is possible, suggesting that design of new vdW interfaces can provide a way to engineer current characteristics of tunneling junctions, including NDR.

II. DEVICE ARCHITECTURE

A general schematic of our vdW-based tunneling transistor is shown in Fig. 1(a). It comprises two electrodes, referred to as "source" and "drain", separated by a thin tunneling barrier. A bias voltage V_b is applied between the two electrodes, while a gate controls an additional voltage V_g. The source electrode consists of two layers arranged in such a way that layer 1, further from the barrier, generates a long-wavelength periodic potential for electrons in layer 2, perturbing their electronic states. In structures involving two-dimensional atomic crystals, such periodic potentials arise naturally as a consequence of different lattice constants of the neighboring materials as well as any misalignment, θ, between their respective crystallographic axes. This leads to the formation of superlattices visually represented by moiré patterns seen, for example, in scanning-tunneling-microscopy measurements [11,12,14–16]. While the impact of the moiré perturbation depends on the atomic composition of the two layers and details of the geometry, in many systems the additional potential leads to Bragg scattering of the electrons and folding of the electronic spectrum into the superlattice Brillouin zone accompanied by the opening of minigaps along its boundary [11–22], as indicated schematically in Fig. 1(b) for the case of graphene on hBN. As a result of such a spectral reconstruction, the electronic DOS is strongly modified—a fact crucial to the functioning of our device as, for a thin tunneling barrier, the current I is sensitive to the source DOS and drain DOS [23], ρ_s and ρ_d, respectively:

$$I = \frac{2g\pi e}{\hbar}\int T(\epsilon)\rho_s(\epsilon)\rho_d(\epsilon-\Delta) \times [f(\epsilon-\mu_s) - f(\epsilon-\Delta-\mu_d)]d\epsilon, \qquad (1)$$

where the energy ϵ is measured from the source charge-neutrality point, μ_s and μ_d determine the energy distance between the chemical potential and the charge-neutrality points in the source electrode and the drain electrode, respectively, Δ is the shift between the source and drain charge-neutrality points such that μ_s and $\mu_d+\Delta$ are the chemical potentials in the corresponding electrodes, T is the transmission coefficient, $f(\epsilon)$ is the Fermi-Dirac distribution (here we take the low-temperature limit), and g takes into account additional degeneracies of the electronic states (here spin and valley). Without the additional moiré modulation, the DOS's of the electrodes usually vary slowly (linearly for monolayer graphene, constant for quasifree electrons in two dimensions) and no NDR is observed [9,10,24] in the absence of momentum-conserving tunneling—this might be the case for devices of insufficient quality or large misalignments between the crystallographic directions of the electrodes. If the momentum-conserving tunneling processes become important, their contribution cannot be larger than the currents discussed here because ultimately the number of tunneling electrons is set by the corresponding DOS, whereas momentum conservation adds an additional constraint that is fulfilled only by some of them.

To relate the energies Δ, μ_s, and μ_d to the applied voltages V_b and V_g, we use the electrostatic relations

$$V_b = \frac{1}{e}(\mu_s-\mu_d-\Delta), \quad \Delta = \frac{e^2 d}{\varepsilon_0\tilde{\varepsilon}}\left[n(\mu_d)+V_g\frac{\varepsilon_0\varepsilon}{ed_g}\right], \qquad (2)$$

where d and d_g are the thickness of the tunneling barrier and the distance between the drain and the back gate, respectively, $\tilde{\varepsilon}$ and ε are the relative permittivities of the barrier and the substrate between the drain and the gate, and $n(\mu_d)$ is the carrier density induced on the drain electrode. In Secs. III and IV, to demonstrate our general idea, we assume that the drain electrode consists of monolayer graphene, so $n(\mu_d) = -\mathrm{sgn}(\mu_d)\mu_d^2/\pi(v\hbar)^2$, with $v\approx 10^6\,\mathrm{m\,s^{-1}}$, the Fermi velocity of the graphene electrons. We also assume that the tunneling barrier is made of thin hBN. As a result, the transmission coefficient T in Eq. (1) depends only weakly on the energy of the initial state, ϵ [24,25], and so we set it to a constant (see the Appendix for a more detailed discussion). As a result, our current is not strictly provided in amperes but is provided in arbitrary units—this, however, is enough to analyze NDR in the proposed devices. Finally, the hBN located in the barrier is rotated by a large angle with respect to the graphene in the source and drain electrodes. Because the impact of the hBN layer on graphene electrons decreases with increasing misalignment angle [11,26], this limits superlattice effects to those generated within the electrodes.

III. GRAPHENE ON HEXAGONAL BN

We first investigate the possibility of superlattice-induced NDR for a source electrode composed of hBN (layer 1) and monolayer graphene (layer 2). As the perturbing effect of hBN on graphene electrons decreases with

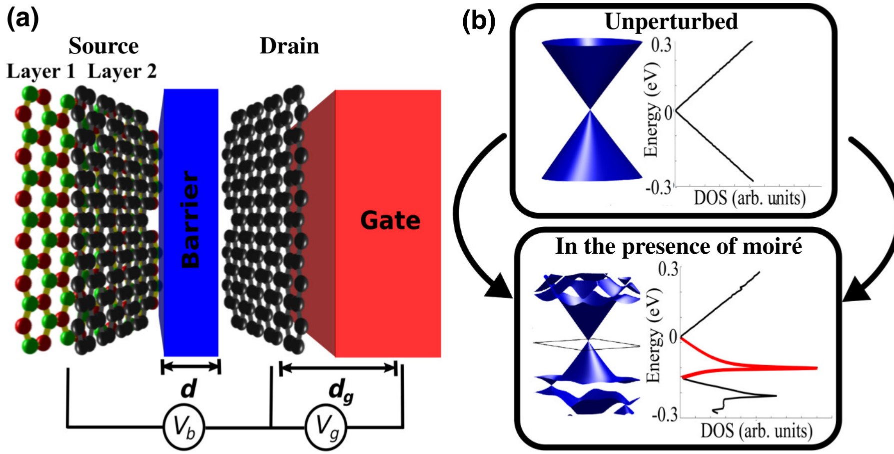

FIG. 1. (a) The tunneling device with a source made of an aligned graphene/hBN heterostructure. Also shown are the distances d and d_g, as well as contacts for voltages V_b and V_g. (b) The conical bands and DOS of unperturbed monolayer graphene (top) and corresponding graphene minibands and DOS of an aligned graphene/hBN heterostructure (bottom). In the miniband spectrum, the black lines indicate the boundaries of a rhombic superlattice Brillouin zone. The Van Hove singularity in the DOS of the heterostructure is highlighted in red.

increasing misalignment between the two crystals [11,26], we assume their crystalline axes are highly aligned. In such a case, the conical dispersion of graphene in the vicinity of the Brillouin-zone corner (valley) is folded into minibands, as indicated in Fig. 1(b), with the valence band undergoing a more significant spectral reconstruction than the conduction band [27], including the appearance of a Van Hove singularity in the DOS [12,27,28], shown in red in Fig. 1(b).

To compute the DOS of the source electrode, we use an interlayer hopping model [27,29,30] for the Hamiltonian of graphene electrons in the valley $\mathbf{K}_\xi = \xi(4\pi/3a, 0)$, $\xi = \pm 1$, perturbed by highly aligned hBN (assuming perfect alignment of the two crystals):

$$\hat{\mathbf{H}}_{G\text{-hBN}} = \hat{\mathbf{H}}_0(\mathbf{p}, 0) + \delta\hat{\mathbf{H}},$$
$$\delta\hat{\mathbf{H}} = V_0\left[\frac{1}{2}f_1(\mathbf{r}) - \xi\frac{\sqrt{3}}{2}\sigma_z f_2(\mathbf{r}) - \frac{\xi}{|\mathbf{b}_0|}[\hat{\mathbf{l}}_z \times \nabla f_1(\mathbf{r})]\cdot\boldsymbol{\sigma}\right],$$
$$f_1(\mathbf{r}) = \sum_{m=0}^{5} e^{i\mathbf{b}_m\cdot\mathbf{r}}, \quad f_2(\mathbf{r}) = i\sum_{m=0}^{5}(-1)^m e^{i\mathbf{b}_m\cdot\mathbf{r}}, \tag{3}$$

written in the basis of $\{\phi_{A,+}, \phi_{B,+}\}^T$ ($\{\phi_{B,-}, -\phi_{A,-}\}^T$) for $\xi = +1$ ($\xi = -1$) of Bloch states $\phi_{i,\xi}$ on one of the sublattices, $i = A, B$, that make up the graphene hexagons, calculated at the center of the valley, $\mathbf{K}_\xi$. Also, we introduce the Pauli matrices σ_x, σ_y, and σ_z, $\boldsymbol{\sigma} = (\sigma_x, \sigma_y)$, acting in the sublattice space, $\mathbf{p} = (p_x, p_y)$ is the momentum of an electron as measured from the center of the valley, and a is the lattice constant of graphene.

The first term in the Hamiltonian, $\hat{\mathbf{H}}_0(\mathbf{p}, \theta) = v e^{i\theta\sigma_z/2}\boldsymbol{\sigma} e^{-i\theta\sigma_z/2}\cdot\mathbf{p}$, describes the low-energy, linear electronic dispersion of unperturbed graphene, while the term $\delta\hat{\mathbf{H}}$ is due to the moiré potential with k-space periodicity given by a set of basic superlattice reciprocal vectors $\mathbf{b}_m = \hat{\mathbf{R}}_{2\pi m/6}[1 - \hat{\mathbf{R}}_\theta/(1+\delta)](0, 4\pi/\sqrt{3}a)$, $m = 0, 1, \ldots, 5$, where $\hat{\mathbf{R}}_\theta$ is the counterclockwise rotation operator and δ is the lattice mismatch (1.8%). The spatial variation of the superlattice potential is described by the two functions $f_1(\mathbf{r})$ and $f_2(\mathbf{r})$, linear combinations of the first harmonics of the moiré, and its strength is characterized by the parameter V_0, which we take equal to 17 meV [22,31].

In Fig. 2(a), we present our simulation of the tunneling current between the graphene/hBN source and graphene drain as a function of the voltages V_b and V_g in a device with hBN as the barrier ($d = 1.3$ nm, $\tilde{\epsilon} = 3$) and a Si gate separated by an insulating layer ($d_g = 180$ nm, $\epsilon = 3.9$), a geometry similar to that in recent experiments [2,3,9,24]. The appearance of NDR can be seen in the top-right quarter in Fig. 2(a), where the tunneling current decreases with increasing bias voltage. We show selected cuts through that region for various constant values of V_g in Fig. 2(b).

For $V_b = V_g = 0$ V, the chemical potentials in the source and drain are located at the respective neutrality points, which are aligned with each other, as in diagram (I) in Fig. 2(c), hence leading to an absence of tunneling current. Applying the bias voltage introduces a relative shift between the source and drain chemical potentials μ_s and $\mu_d + \Delta$, respectively. As a result, an increase in V_b for $V_g = 0$ V [corresponding to following the dashed orange line in Figs. 2(a) and 2(b)] leads to an increasing current as electrons from the valence band in the source can tunnel into the empty conduction-band states of the drain. For V_b slightly above 0.2 V, $\mu_d + \Delta$ moves past the moiré-induced Van Hove singularity in the source valence band, which leads to a shoulderlike feature in the orange curve in Fig. 2(b).

In contrast, applying the gate voltage V_g at constant V_b dopes the source and drain without affecting the energy difference between the chemical potentials, μ_s and $\mu_d + \Delta$. As shown in diagram (II) in Fig. 2(c), for $V_g = 40$ V and $V_b = 0$ V no current flows through the structure because the chemical potentials are aligned, as in diagram (I).

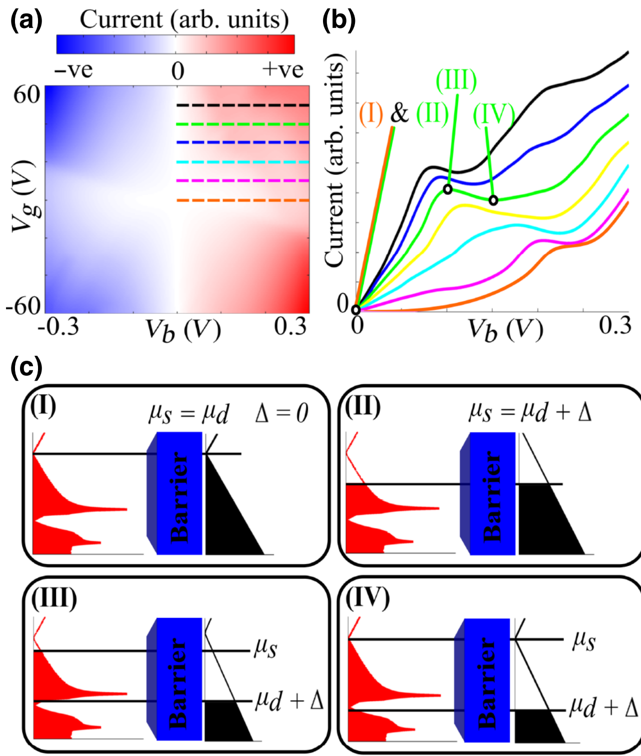

FIG. 2. (a) Calculated tunneling current for a device from Fig. 1(a) as a function of voltages V_g and V_b. (b) Tunneling current as a function of V_b for constant V_g from 0 V (orange) to 50 V (black) in steps of 10 V. The cuts in (V_g, V_b) space corresponding to current curves in (b) are shown with dashed lines in (a). (c) Diagrams showing alignment of source DOS and drain DOS as well as the positions of chemical potentials μ_s and $\mu_d + \Delta$ for points in (V_g, V_b) space corresponding to tunneling currents marked as (I), (II), (III), and (IV) in (b).

Again, the current increases with increasing bias [as demonstrated by the green curve in Fig. 2(b)] until it reaches a peak when the occupied states in the moiré-induced Van Hove singularity are aligned with empty states in the drain valence band, as in diagram (III). Because the Van Hove singularity in the source DOS is followed by a dip, increasing V_b further does not lead to more occupied electronic states contributing to the tunneling. However, because changing V_b affects the energy shift Δ between the Dirac points of the source and the drain through Eq. (2), the number of empty states aligned with the Van Hove singularity actually decreases with increasing V_b, as seen by comparing diagrams (III) and (IV). This results in a decrease of the current and NDR.

IV. TWISTED-BILAYER GRAPHENE

To demonstrate the generality of our idea, we now discuss the existence of NDR in a tBLG/hBN/monolayer graphene vdW tunneling transistor. Twisted-bilayer graphene [15,32–36] comprises two stacked and rotationally misaligned graphene sheets. Because, in contrast to graphene on highly aligned hBN, in tBLG both layers have the same lattice constant, rotational misalignment is necessary to form a moiré superlattice. As a result of the twist, the interlayer coupling depends on the position **r** within the crystal, leading to an effective Hamiltonian [37–39]

$$\hat{\mathbf{H}}_{\text{tBLG}} = \begin{pmatrix} \hat{\mathbf{H}}_0(\mathbf{p}, -\frac{\theta}{2}) + \frac{u}{2} & \hat{\mathbf{T}}^\dagger(\theta) \\ \hat{\mathbf{T}}(\theta) & \hat{\mathbf{H}}_0(\mathbf{p}, \frac{\theta}{2}) - \frac{u}{2} \end{pmatrix},$$

$$\hat{\mathbf{T}}(\theta) = \frac{\gamma_1}{3} \sum_{j=0}^{2} e^{i\hat{R}_{2\pi j/3}\Delta\mathbf{K}\cdot\mathbf{r}} \begin{pmatrix} 1 & \xi e^{-ij2\pi/3} \\ \xi e^{ij2\pi/3} & 1 \end{pmatrix}, \quad (4)$$

where we include the effect of the electric field between the layers by introducing an on-site potential-energy difference between the layers, u, related to the applied gate voltage:

$$u = \frac{e^2 d_0}{\varepsilon_0} \left[n(\mu_d) + \frac{1}{2} n(\mu_s, u) + V_g \frac{\varepsilon_0 \varepsilon}{e d_g} \right], \quad (5)$$

where $d_0 = 0.33$ nm is the bilayer-graphene interlayer distance. The Hamiltonian in Eq. (4), written in the basis of $\{\phi_{A1,+}, \phi_{B1,+}, \phi_{A2,+}, \phi_{B2,+}\}^T$ $(\{\phi_{B1,-}, -\phi_{A1,-}, \phi_{B2,-}, -\phi_{A2,-}\}^T)$ for $\xi = +1$ $(\xi = -1)$, describes hybridization of the two Dirac cones displaced by a vector $\Delta\mathbf{K} \approx 2|\mathbf{K}_\xi| \sin(\theta/2)(0, -1)$ from one another. Midway between the cones, repulsion between two crossing linear dispersions leads to the opening of a local gap and the appearance of a peak in the DOS, as shown in Fig. 3(a). This peak has been observed by scanning tunneling microscopy [15] and is known to modify the optical conductivity [33,34] and Raman spectra [32] of tBLG. Unlike in Bernal-stacked bilayer graphene [40], u does not open a band gap in tBLG but instead leads to small changes in the energy position of the Dirac cones of each layer. We compute u self-consistently assuming that the charge density is equally distributed between the two layers. The overall impact of u on the DOS is small, and all features in the current-voltage maps can be qualitatively explained with $u = 0$.

For our modeling of the tunneling between tBLG and graphene across a hBN multilayer, we choose the misalignment angle 2°, corresponding to the low-energy band structure in the vicinity of a single valley and DOS as shown in Fig. 3(a). All the other geometrical parameters of the device are as used in the case of the graphene/hBN source electrode. The calculated current as a function of the bias and gate voltages V_b and V_g is shown in Fig. 3(b) and selected cuts for constant V_g are presented in Fig. 3(c). Similarly to the case of the graphene/hBN electrode, superlattice-induced spectral reconstruction, in particular, the presence of sharp Van Hove singularities followed by a dip, leads to NDR for a range of gate voltages.

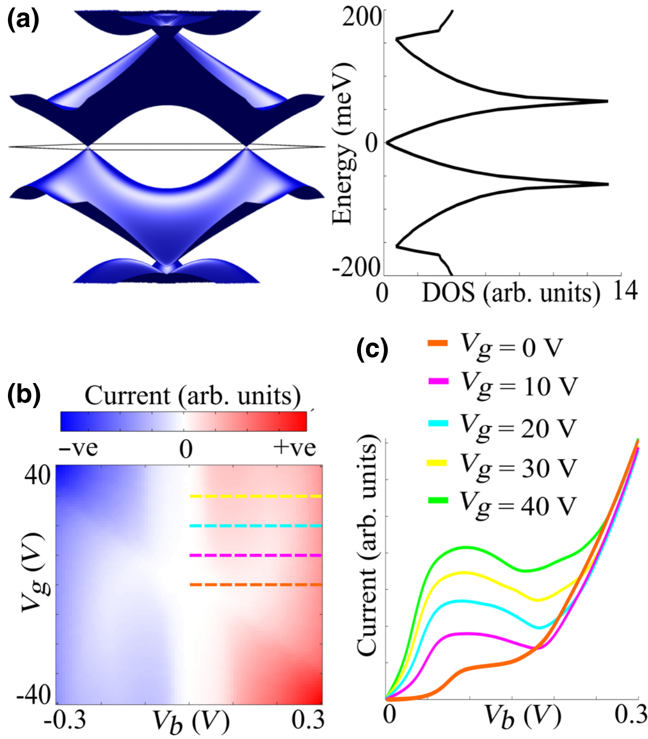

FIG. 3. (a) Low-energy band structure and DOS for tBLG with a misalignment angle of 2°. Note that both the position and the height of the Van Hove singularity change with misalignment angle. The black line indicates the superlattice Brillouin-zone edge. (b) Tunneling current from tBLG to graphene across a hBN barrier as a function of gate and bias voltages V_g and V_b. (c) Tunneling current as a function of V_b for constant V_g from 0 V (orange) to 40 V (green) in steps of 10 V. The cuts in (V_b, V_g) space corresponding to the current curves in (c) are shown with dashed lines in (b).

Because the Van Hove singularity is a robust feature in the DOS of tBLG for a large range of misalignment angles [21], the behavior of the tunneling current should also be similar for different θ (although note that greater misalignment angle requires higher V_g to dope the source past the singularity). Also, because, in contrast to the aligned graphene/hBN heterostructure, the DOS of tBLG is electron-hole symmetric, the graph in Fig. 3(b) is inversion symmetric with respect to the point $V_b = V_g = 0$ V.

V. GRAPHENE ON α-In_2Te_2

While the architectures discussed in Secs. III and IV demonstrate the principle of moiré-induced NDR and are feasible experimentally, the calculated NDR peak-to-valley ratio is only of order 1. One can increase it by choosing a different vdW heterostructure as an electrode, in particular, one with a moiré reconstructed DOS in which a band gap between minibands is close to a Van Hove singularity. Moreover, designing superlattices to modulate the densities of states of both electrodes as opposed to use of monolayer graphene with its linear DOS as a drain as in the two examples earlier will also increase NDR.

Hence, in this section, we investigate current characteristics of a vdW tunneling transistor with both electrodes made of graphene on α-In_2Te_2. It was proposed that such a heterostructure would belong to a group for which the moiré pattern results from the beating between the lattice constants of α-In_2Te_2 and the lattice constant of a tripled graphene unit cell, $\sqrt{3}a$ [41,42], with the mismatch between the two, δ', approximately -0.7% [43,44]. It was predicted [41], in this case, that the arising moiré potential would lead to a periodically-oscillating-in-space intervalley coupling for graphene electrons, captured by the Hamiltonian

$$\begin{aligned}
\hat{\mathbf{H}}_{G\text{-}\sqrt{3}} &= \hat{\mathbf{H}}_0(\mathbf{p},0) + \delta\hat{\mathbf{H}}',\\
\delta\hat{\mathbf{H}}' &= V_0'\left[\frac{1}{2}F(\mathbf{r}) - \frac{1}{|\boldsymbol{\beta}_0|}[\boldsymbol{\sigma}\times\hat{\mathbf{l}}_z]\cdot\nabla F(\mathbf{r})\right],\\
f_1(\mathbf{r}) &= \sum_{m=0}^{5} e^{i\boldsymbol{\beta}_{\rm m}\cdot\mathbf{r}}, \quad f_2(\mathbf{r}) = i\sum_{m=0}^{5}(-1)^m e^{i\boldsymbol{\beta}_{\rm m}\cdot\mathbf{r}},\\
F(\mathbf{r}) &= \tau_x f_1(\mathbf{r}) + \tau_y f_2(\mathbf{r}),
\end{aligned} \tag{6}$$

written in the basis $\{\phi_{A,+},\phi_{B,+},\phi_{B,-},\phi_{-A,-}\}^T$ with Pauli matrices τ_x, τ_y acting in the valley space and a set of reciprocal space vectors $\boldsymbol{\beta}_m = (1/\sqrt{3})\hat{\mathbf{R}}_{-\pi/2}\mathbf{b}_m$, $m = 0,1,\ldots,5$. As for graphene on hBN, the term $\delta\hat{\mathbf{H}}'$ describes the contribution due to the moiré potential, with V_0' setting its strength. We assume that the interlayer interactions in graphene/α-In_2Te_2 are comparable to those in graphene/hBN and so use $V_0' = V_0 = 17$ meV for our calculations. The calculated miniband spectrum is shown in Fig. 4(a). Notice that, in contrast to the miniband spectra discussed for graphene on hBN in Sec. II, this spectrum displays flat bands around zero energy, similarly to magic-angle tBLG [35,36], with small band gaps separating them from the rest of the spectrum. This leads to a DOS as shown in Fig. 4(b), containing Van Hove singularities next to a window of zero DOS, features attractive for an increased NDR. In Fig. 4(c), we present the current calculated as a function of the gate and bias voltages for a vdW tunneling transistor incorporating graphene/α-In_2Te_2 heterostructures as both the source and the drain (all other parameters of the device are kept the same as in Secs. II and III). Current curves for selected constant gate voltages and changing bias are shown in Fig. 4(d) (region of positive V_g and V_b) and Fig. 4(e) (region of negative V_g and V_b). For easier comparison with other figures in this paper, we reverse the current and bias-voltage axes in Fig. 4(e). Moreover, the current scale in Fig. 4(d) is scaled by a factor of 3 as compared with Fig. 4(e).

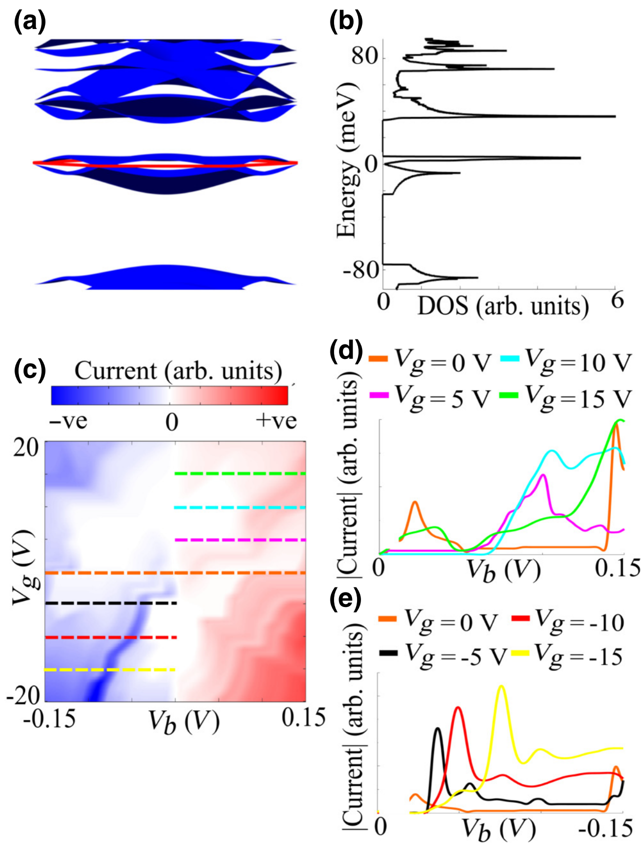

FIG. 4. (a) Low-energy band structure of graphene on aligned α-In_2Te_2. The outline of the superlattice Brillouin zone is shown in red for clarity. (b) Corresponding DOS. (c) Tunneling current between two graphene-on-aligned-α-In_2Te_2 electrodes across a hBN barrier as a function of gate and bias voltages V_g and V_b. (d) Absolute tunneling current as a function of V_b for constant V_g from 0 V (orange) to 15 V (green) in steps of 5 V. The cuts in (V_b, V_g) space corresponding to the current curves in (d) are shown with dashed lines in (c). The current lines in (d) are scaled to highlight NDR features. (e) Same as (d) except for negative gate and bias voltages with steps of -5 V from 0 V (orange) to -15 V (yellow).

All of the current-voltage characteristics in Figs. 4(d) and 4(e) show NDR peak-to-valley ratios ranging from 2 to 10, depending on the choice of gate voltage. The largest NDR of around 10 is for $V_g = 0$ V (orange curve) in Fig. 4(d). It results from the presence of two Van Hove singularities in the DOS around zero energy [see Fig. 4(b)] and their movement on the energy scale in the source and drain electrodes as a function of V_b.

VI. SUMMARY

In summary, we demonstrate theoretically for three different architectures that the modifications of the electronic DOS due to the formation of moiré superlattices of vdW crystals can lead to NDR when the moiré heterostructure is used as an electrode in a vertical tunneling transistor. This is achieved without the requirement of momentum-conserving tunneling, which has been observed only in the highest-quality, closely aligned devices made of mechanically exfoliated crystals. For this reason, our idea might be useful for materials produced by other methods, such as chemical vapor deposition, where clear moiré reconstruction has been observed [15,45] but no momentum-conserving tunneling has been reported. While the moiré superlattices used in the first two examples, graphene on hBN and tBLG, have been realized experimentally, the last one, graphene on α-In_2Te_2, has not. However, superlattice effects have been observed or predicted for a variety of different heterostructures and interfaces [42,46–48], so a significant NDR peak-to-valley ratio might indeed be possible for certain architectures, as suggested in Sec. V. Importantly, in contrast to artificial superlattices, our idea avoids the need to process any of the two-dimensional crystals after they are grown, as the superlattice is provided by an interface between neighboring layers. This, in turn, limits disorder and degradation of the components, which is especially important if the starting materials were not obtained by mechanical exfoliation. In contrast to many other NDR setups, our idea is, by design, easy to integrate in more-complicated devices based on two-dimensional crystals and vdW interfaces. It can also be coupled with artificial patterning of dielectric substrates underneath two-dimensional materials on length scales comparable to moiré wavelengths [49].

ACKNOWLEDGMENTS

This work has been supported by the UK Engineering and Physical Sciences Research Council (EPSRC) through the University of Bath Doctoral Training Partnership, EPSRC Grant No. EP/M50645X/1 and EPSRC Grant No. EP/M507982/1.

D.J.L. and J.J.P.T. contributed equally to this work.

APPENDIX: ENERGY DEPENDENCE OF TRANSMISSION COEFFICIENT

For thin, strongly insulating tunneling barriers (such as hBN), the transmission coefficient T depends only weakly on the energy of the initial state, ϵ [24,25], and so we set it to a constant in the main text for ease of analysis. In general, the variation in the barrier height $\Phi(\epsilon)$ due to changing electron kinetic energy leads to a modification of the decay constant k, which becomes a function of ϵ and so does the transmission coefficient, which decreases exponentially with barrier thickness, d:

$$T(\epsilon) = \exp[-k(\epsilon)d]. \quad \text{(A1)}$$

Assuming graphene electrodes, the multilayer-hBN barrier can be treated as an isotropic potential step [24] with barrier height $\Phi_0 = -1.5$ eV, corresponding to previous measurements of the valence-band maximum of hBN [24,25]. Approximating hBN energy bands as roughly parabolic around the valence-band maximum allows us to write [50]

$$k(\epsilon) = \mathrm{Im}\frac{\sqrt{2m^*\Phi(\epsilon)}}{\hbar} = \mathrm{Im}\frac{\sqrt{2m^*(\Phi_0 - \epsilon)}}{\hbar}, \qquad \text{(A2)}$$

where $m^* \approx 0.5m_0$ is the effective mass [24,25]. Notably, this predicts electron-hole asymmetry in tunneling current as observed in experiments [24,25].

Application of this varying tunneling coefficient to our model increases the tunneling current and conductance in the conduction-band-to-conduction-band regions and reduces the current and conductance in the valence-band-to-valence-band regions. Crucially, all NDR features shown in our calculations still persist, with conduction-band peak-to-valley ratio slightly increased and valence-band peak-to-valley ratio slightly decreased in all systems discussed in the main text. Increasing the tunneling-barrier thickness or using a less-insulating material such as WS_2 [25] would require the potential modulation of the transmission coefficient to be included so as to give accurate results. However, despite the observation that across the voltage range investigated the transmission coefficient varies noticeably, locally, around the current peak and valley voltages, the transmission coefficient is roughly constant, and so all NDR features that we predict will persist.

In a general formalism, determining the tunneling current requires finding the overlap between the relevant electron wave functions on the electrodes. This can be decomposed into a term describing the transverse component of the overlap, $T(\epsilon)$, and an in-plane momentum-conserving component, which is constant for momentum-nonconserving tunneling. In real devices, the total current is a sum of all tunneling processes, both conserving momentum and not conserving momentum. However, as mentioned in the main text, the upper bounds on the current are set by the available initial and final DOS, so any contributions not considered here cannot be larger than those we discuss in the main text. The arbitrariness of our unit of current in Figs. 2–4 originates in our setting $T(\epsilon)$ to an unspecified constant, which affects any other tunneling process in the same way.

[1] L. Esaki, New phenomenon in narrow germanium para-normal-junctions, Phys. Rev. **109**, 603 (1958).

[2] L. Britnell, R. V. Gorbachev, A. K. Geim, L. A. Ponomarenko, A. Mishchenko, M. T. Greenaway, T. M. Fromhold, K. S. Novoselov, and L. Eaves, Resonant tunnelling and negative differential conductance in graphene transistors, Nat. Comms. **4**, 1794 (2013).

[3] A. Mishchenko, J. S. Tu, Y. Cao, R. V. Gorbachev, J. R. Wallbank, M. T. Greenaway, V. E. Morozov, S. V. Morozov, M. J. Zhu, S. L. Wong, F. Withers, C. R. Woods, Y. J. Kim, K. Watanabe, T. Taniguchi, E. E. Vdovin, O. Makarovsky, T. M. Fromhold, V. I. Fal'ko, A. K. Geim, L. Eaves, and K. S. Novoselov, Twist-controlled resonant tunnelling in graphene/boron nitride/graphene heterostructures, Nat. Nano **9**, 808 (2014).

[4] B. Fallahazad, K. Lee, S. Kang, J. M. Xue, S. Larentis, C. Corbet, K. Kim, H. C. P. Movva, T. Taniguchi, K. Watanabe, L. F. Register, S. K. Banarjee, and E. Tutuc, Gate-tunable resonant tunneling in double bilayer graphene heterostructures, Nano Lett. **15**, 428 (2015).

[5] S. Kang, B. Fallahazad, K. Lee, H. Movva, K. Kim, C. M. Corbet, T. Taniguchi, K. Watanabe, L. Colombo, L. F. Register, E. Tutuc, and S. K. Banerjee, Bilayer graphene-hexagonal boron nitride heterostructure negative differential resistance interlayer tunnel FET, IEEE Electron Device Lett. **36**, 405 (2015).

[6] K. Kim, M. Yankowitz, B. Fallahazad, S. Kang, H. C. P. Movva, S. Q. Huang, S. Larentis, C. M. Corbet, T. Taniguchi, K. Watanabe, S. K. Banerjee, B. J. LeRoy, and E. Tutuc, Van der Waals Heterostructures with high accuracy rotational alignment, Nano Lett. **16**, 1989 (2016).

[7] J. R. Wallbank, D. Ghazaryan, A. Misra, Y. Cao, J. S. Tu, B. A. Piot, M. Potemski, S. Pezzini, S. Wiedmann, U. Zietler, T. L. M. Lane, S. V. Morozov, M. T. Greenaway, L. Eaves, A. K. Geim, V. I. Fal'ko, K. S. Novoselov, and A. Mishchenko, Tuning the valley and chiral quantum state of Dirac electrons in Van der Waals heterostructures, Science **353**, 575 (2016).

[8] S. J. Haigh, A. Gholinia, R. Jalil, S. Romani, L. Britnell, D. C. Elias, K. S. Novoselov, L. A. Ponomarenko, A. K. Geim, and R. Gorbachev, Cross-sectional imaging of individual layers, buried interfaces of graphene-based heterostructures, superlattices, Nat. Mat. **11**, 764 (2012).

[9] S. H. Lee, M. S. Choi, J. Lee, C. H. Ra, X. Liu, E. Hwang, J. H. Choi, J. Q. Zhong, W. Chen, and W. J. Yoo, High performance vertical tunneling diodes using graphene/hexagonal boron nitride/graphene hetero-structure, Appl. Phys. Lett. **104**, 053103 (2014).

[10] T. Roy, L. Liu, S. de la Barrera, B. Chakrabarti, Z. R. Hesabi, C. A. Joiner, R. M. Feenstra, G. Gu, and E. M. Vogel, Tunneling characteristics in chemical vapor deposited graphene-hexagonal boron nitride-graphene junctions, Appl. Phys. Lett. **104**, 123506 (2014).

[11] M. Yankowitz, J. M. Xue, D. Cormode, J. D. Sanchaz-Yamagishi, K. Watanabe, T. Taniguchi, P. Jarillo-Herrero, P. Jacquod, and B. J. LeRoy, Emergence of superlattice Dirac points in graphene on hexagonal boron nitride, Nat. Phys. **8**, 382 (2012).

[12] E. Y. Wang, X. B. Lu, S. J. Ding, W. Yao, M. Z. Yan, G. L. Wan, K. Deng, S. P. Wang, G. R. Chen, L. G. Ma, J. Jung, A. V. Fedorov, Y. B. Zhang, G. Y. Zhang, and S. Y. Zhou, Gaps induced by inversion symmetry breaking and second-generation Dirac cones in graphene/hexagonal boron nitride, Nat. Phys. **12**, 1111 (2016).

[13] Z. W. Shi, C. H. Jin, W. Yang, L. Ju, J. Horng, X. B. Lu, H. A. Bechtel, M. C. Martin, D. Y. Fu, J. Q. Wu, K. Watanabe, T. Taniguchi, Y. B. Zhang, X. D. Bai, E. G. Wang, G. Y. Zhang, and F. Wang, Gate-dependent pseudospin mixing in graphene/boron nitride moire superlattices, Nat. Phys. **10**, 743 (2014).

[14] W. Yang, X. Lu, G. Chen, S. Wu, G. B. Xie, M. Cheng, D. M. Wang, R. Yang, D. X. Shi, K. Watanabe, T. Taniguchi, C. Voisin, B. Placais, Y. B. Zhang, and G. Y. Zhang, Hofstadter Butterfly and Many-Body Effects in Epitaxial Graphene Superlattice, Nano Lett. **16**, 2387 (2016).

[15] G. H. Li, A. Luican, J. M. B. L. dos Santos, A. H. Castro Neto, A. Reina, J. Kong, and E. Y. Andrei, Observation of Van Hove singularities in twisted graphene layers, Nat. Phys. **6**, 109 (2010).

[16] W. Yan, M. X. Liu, R. F. Dou, L. Meng, L. Feng, Z. D. Chu, Y. F. Zhang, Z. F. Liu, J. C. Nie, and L. He, Angle-Dependent van Hove Singularities in a Slightly Twisted Graphene Bilayer, Phys. Rev. Lett. **109**, 126801 (2012).

[17] Z. J. Tan, J. Yin, C. Chen, H. Wang, L. Lin, L. Z. Sun, J. X. Wu, X. Sun, H. F. Yang, Y. L. Chen, H. L. Peng, and Z. F. Liu, Building Large-domain twisted bilayer graphene with van Hove singularity, ACS Nano **10**, 6725 (2016).

[18] Y. Kim, P. Herlinger, P. Moon, M. Koshino, T. Taniguchi, K. Watanabe, and J. H. Smet, Charge inversion and topological phase transition at a twist angle induced van Hove singularity of bilayer graphene, ACS Nano **16**, 5053 (2016).

[19] D. Pierucci, H. Henck, J. Avila, A. Balan, C. H. Naylor, G. Patriarche, Y. J. Dappe, M. G. Silly, F. Sirotti, A. T. C. Johnson, M. C. Asensio, and A. Ouerghi, Band alignment and minigaps in monolayer MoS^2-graphene van der Waals heterostructures, Nano Lett. **16**, 4054 (2016).

[20] E. Koren, I. Leven, E. Lortscher, A. Knoll, O. Hod, and U. Duerig, Coherent commensurate electronic states at the interface between misoriented graphene layers, Nat. Nano **11**, 752 (2016).

[21] I. Brihuega, P. Mallet, H. Gonzalez-Herrero, G. T. de Laissardiere, M. M. Ugeda, L. Magaud, J. M. Gomez-Rodriguez, F. Yndurain, and J. Y. Veuillen, Unraveling the Intrinsic and Robust Nature of van Hove Singularities in Twisted Bilayer Graphene by Scanning Tunneling Microscopy and Theoretical Analysis, Phys. Rev. Lett. **109**, 196802 (2012).

[22] M. Lee, J. R. Wallbank, P. Gallagher, K. Watanabe, T. Taniguchi, V. I. Fal'ko, and D. Goldhabor-Gordon, Ballistic miniband conduction in a graphene superlattice, Science **353**, 1526 (2016).

[23] P. Moffatt and E. H. Kim, Negative differential resistance from a van Hove singularity in tunnel diodes, Appl. Phys. Lett. **89**, 192117 (2006).

[24] L. Britnell, R. V. Gorbachev, R. Jalil, B. D. Belle, F. Schedin, A. Mishchenko, T. Georgiou, M. I. Katnelson, L. Eaves, S. V. Morozov, N. M. R. Peres, J. Leist, A. K. Geim, K. S. Novoselov, and L. A. Ponomarenko, Field-effect tunneling transistor based on vertical graphene heterostructures, Science **335**, 947 (2012).

[25] T. Georgiou, R. Jalil, B. D. Belle, L. Britnell, R. V. Gorbachev, S. V. Morozov, Y. J. Kim, A. Gholinia, S. J. Haigh, O. Makarovsky, L. Eaves, L. A. Ponomarenko, A. K. Geim, K. S. Novoselov, and A. Mishchenko, Vertical field-effect transistor based on graphene-WS_2 heterostructures for flexible and transparent electronics, Nat. Nano **8**, 100 (2013).

[26] J. Jung, E. Laksono, A. M. DaSilva, A. H. MacDonald, M. Mucha-Kruczyński, and S. Adam, Moiré band model and band gaps of graphene on hexagonal boron nitride, Phys. Rev. B **96**, 085442 (2017).

[27] J. R. Wallbank, A. A. Patel, M. Mucha-Kruczyński, A. K. Geim, and V. I. Fal'ko, Generic miniband structure of graphene on a hexagonal substrate, Phys. Rev. B **87**, 245408 (2013).

[28] M. Mucha-Kruczyński, J. R. Wallbank, and V. I. Fal'ko, Moiré miniband features in the angle-resolved photoemission spectra of graphene/hBN heterostructures, Phys. Rev. B **93**, 085409 (2016).

[29] J. R. Wallbank, M. Mucha-Kruczyński, X. Chen, and V. I. Fal'ko, Moiré miniband features in the angle-resolved photoemission spectra of graphene/hBN heterostructures, Ann. Phys. **527**, 359 (2015).

[30] M. Kindermann, B. Uchoa, and D. L. Miller, Zero-energy modes and gate-tunable gap in graphene on hexagonal boron nitride, Phys. Rev. B **86**, 115415 (2012).

[31] G. X. Ni, H. Wang, J. S. Wu, Z. Fei, M. D. Goldflam, F. Keilmann, B. Õzyilmaz, A. H. Castro Neto, X. M. Xie, M. M. Fogler, and D. N. Basov, Plasmons in graphene moire superlattices, Nat. Mater. **14**, 1217 (2015).

[32] K. Kim, S. Coh, L. Z. Tan, W. Regen, J. M. Yuk, E. Chatterje, M. F. Crommie, M. L. Cohen, S. G. Louie, and A. Zettl, Raman Spectroscopy Study of Rotated Double-Layer Graphene: Misorientation-Angle Dependence of Electronic Structure, Phys. Rev. Lett. **108**, 246103 (2012).

[33] J. T. Robinso, S. W. Schmucker, C. B. Diaconescu, J. P. Long, J. C. Culbertson, T. Ohta, A. L. Friedman, and T. E. Beechem, Electronic hybridization of large-area stacked graphene films, ACS Nano **7**, 637 (2013).

[34] J. Campos-Delgado, G. Algara-Siller, C. N. Santos, U. Kaiser, and J. P. Raskin, Twisted bi-layer graphene: Microscopic rainbows, Small **9**, 3247 (2013).

[35] Y. Cao, V. Fatemi, A. Demir, S. Fang, S. L. Tomarken, J. Y. Luo, J. D. Sanchez-Yamagishi, K. Watanabe, T. Taniguchi, E. Kaxiras, R. C. Ashoori, and P. Jarillo-Herrero, Correlated insulator behaviour at half-filling in magic-angle graphene superlattices, Nature **556**, 80 (2018).

[36] Y. Cao, V. Fatemi, S. Fang, K. Watanabe, T. Taniguchi, E. Kaxiras, and P. Jarillo-Herrero, Unconventional superconductivity in magic-angle graphene superlattices, Nature **556**, 43 (2018).

[37] J. M. B. Lopes dos Santos, N. M. R. Peres, and A. H. Castro, Graphene Bilayer with a Twist: Electronic Structure, Phys. Rev. Lett. **99**, 256802 (2007).

[38] R. Bistritzer and A. H. MacDonald, Moiré bands in twisted double-layer graphene, Proc. Nat. Acad. Sci. USA **108**, 12233 (2011).

[39] E. J. Mele, Band symmetries and singularities in twisted multilayer graphene, Phys. Rev. B **84**, 235439 (2011).

[40] E. McCann and V. I. Fal'ko, Landau-Level Degeneracy and Quantum Hall Effect in a Graphite Bilayer, Phys. Rev. Lett. **96**, 086805 (2006).

[41] J. R. Wallbank, M. Mucha-Kruczyński, and V. I. Fal'ko, Moiré minibands in graphene heterostructures with almost commensurate $\sqrt{3} \times \sqrt{3}$ hexagonal crystals, Phys. Rev. B **88**, 155415 (2013).

[42] D. J. Leech and M. Mucha-Kruczyński, Controlled formation of an isolated miniband in bilayer graphene on an almost commensurate $\sqrt{3} \times \sqrt{3}$ substrate, Phys. Rev. B **94**, 165437 (2016).

[43] V. Zolyomi, N. D. Drummond, and V. I. Fal'ko, Electrons and phonons in single layers of hexagonal indium chalcogenides from Ab initio calculations, Phys. Rev. B **89**, 205416 (2014).

[44] G. Giovannetti, M. Capone, J. van den Brink, and C. Ortix, Kekulé textures, pseudospin-one Dirac cones, and quadratic band crossings in a graphene-hexagonal indium chalcogenide bilayer, Phys. Rev. B **91**, 121417 (2015).

[45] D. Wong, Y. Wang, J. Jung, S. Pezzini, A. M. DaSilva, H. Tsai, H. S. Jung, R. Khajeh, Y. Kim, J. Lee, S. Kahn, S. Tollabimazraehno, H. Rasool, K. Watanabe, T. Taniguchi, A. Zettl, S. Adam, A. H. MacDonald, and M. F. Crommie, Local spectroscopy of moiré-induced electronic structure in gate-tunable twisted bilayer graphene, Phys. Rev. B. **92**, 155409 (2015).

[46] Q. Tong, H. Y. Yu, Q. Z. Zhu, Y. Wang, X. D. Xu, and A. Yao, Topological Mosaics in Moiré Superlattices of van der Waals Heterobilayers, Phys. Rev. Lett. **13**, 356 (2017).

[47] C. D. Zhang, C. P. Chuu, X. B. Ren, L. J. Li, C. H. Jin, M. Y. Chou, and C. K. Shih, Interlayer couplings, moiré patterns, and 2D electronic superlattices in MoS_2/WSe_2 hetero-bilayers, Sci. Adv. **3**, 1601459 (2017).

[48] Y. Pan, S. Fölsch, Y. Nie, D. Waters, Y. C. Li, B. Jariwala, K. Zhang, K. Cho, J. A. Robinson, and R. M. Feenstra, Quantum-confined electronic states arising from the moiré pattern of MoS_2-WSe_2 heterobilayers, Nano Lett. **18**, 1849 (2018).

[49] C. Forsythe, X. Zhou, T. Taniguchi, K. Watanabe, A. Pasupathy, P. Moon, M. Koshino, P. Kim, and C. R. Dean, Band structure engineering of 2D materials using patterned dielectric superlattices, Nat. Nano **13**, 566 (2018).

[50] J. G. Simmons, Formula for the electric tunnel effect between similar electrodes separated by a thin insulating film, Jour. App. Phys. **34**, 1793 (1963).